Mon. Not. R. Astron. Soc. **000**, 000–000 (0000) Printed 8 March 2007 (MN LATEX style file v2.2)

The Observed Concentration-Mass Relation for Galaxy Clusters

Julia M. Comerford[1] and Priyamvada Natarajan[2,3]
[1]*Astronomy Department, 601 Campbell Hall, University of California, Berkeley, CA 94720-3411*
[2]*Department of Astronomy, Yale University, P.O. Box 208101, New Haven, CT 06520-8101*
[3]*Department of Physics, Yale University, P.O. Box 208120, New Haven, CT 06520-8120*

8 March 2007

ABSTRACT
The properties of clusters of galaxies offer key insights into the assembly process of structure in the universe. Numerical simulations of cosmic structure formation in a hierarchical, dark matter dominated universe suggest that galaxy cluster concentrations, which are a measure of a halo's central density, decrease gradually with virial mass. However, cluster observations have yet to confirm this correlation. The slopes of the run of measured concentrations with virial mass are often either steeper or flatter than predicted by simulations. In this work, we present the most complete sample of observed cluster concentrations and masses yet assembled, including new measurements for 10 strong lensing clusters, thereby more than doubling the existing number of strong lensing concentration estimates. We fit a power law to the observed concentrations as a function of virial mass, and find that the slope is consistent with the slopes found in simulations, though our normalization factor is higher. Observed lensing concentrations appear to be systematically larger than X-ray concentrations, a more pronounced effect than found in simulations. We also find that at fixed mass, the bulk of observed cluster concentrations are distributed log-normally, with the exception of a few anomalously high concentration clusters. We examine the physical processes likely responsible for the discrepancy between lensing and X-ray concentrations, and for the anomalously high concentrations in particular. The forthcoming Millennium simulation results will offer the most comprehensive comparison set to our findings of an observed concentration-mass power law relation.

Key words: cosmology: observations – dark matter – gravitational lensing – galaxies: clusters: general

1 INTRODUCTION

Galaxy clusters are the most recent structures to assemble in a hierarchical ΛCDM universe and therefore offer important clues to the detailed understanding of the growth of structure in the universe. The ΛCDM paradigm is well studied and observationally supported on the largest scales by the cosmic microwave background data, high-z supernovae, and galaxy surveys. Clusters of galaxies are a useful laboratory to further test this paradigm, as their masses, abundances, and other properties such as baryon fraction provide key cosmological constraints.

Clusters also provide overwhelming evidence for the existence of copious amounts of dark matter in the universe. The bulk of the mass of a cluster is dark matter ($\sim 85\%$), with hot baryonic gas contributing about 10% and the rest provided by the stellar content of the constituent galaxies.

One of the key predictions of CDM is the excellent fit to density profiles on a wide range of scales provided by the Navarro-Frenk-White (NFW) form (Navarro et al. 1996, 1997), or with modifications to the inner slope (Moore et al. 1999; Navarro et al. 2004). In numerical simulations of structure formation, it is found that this profile fits dwarf galaxy scale dark matter halos as well as massive, cluster scale dark matter halos. For a typical cluster dark matter halo in these simulations, the density profile steepens for radii larger than the halo's typical scale radius (defined more precisely in § 2 below).

A useful diagnostic, the halo concentration, can be defined as the ratio of the halo's virial radius to its scale radius. This concentration parameter reflects the central density of the halo, which depends on the halo's assembly history and thereby on its time of formation. Since in the hierarchical structure formation scenario massive galaxy clusters are the most recent bound objects to form, their concentrations are a crucial probe of the mean density of the universe at relatively late epochs.

As originally suggested by Navarro et al. (1996) and supported by later numerical simulations of cosmological structure formation (Bullock et al. 2001; Hennawi et al. 2007), a halo's concentration parameter is related to its virial mass, with the concentration decreasing gradually with mass. Given this prediction it is important to test this trend with observational data, as this offers an indirect check on the veracity of the paradigm itself. The situation at present with observed clusters with measured concentrations is unclear due to the plurality of methods employed to derive these

concentrations as well as systematics arising from the complex dynamics and its effect on mass distributions.

In this paper, we present new concentration measurements for 10 strong lensing clusters and combine our results with other measurements in the literature to construct an observed concentration-mass relation for galaxy clusters. In § 2, we present the basic definitions and equations relevant to computing concentrations. In the following section, § 3, we define the observational sample and the various methods used to select these clusters. We present the constructed observed concentration-mass relation in § 4, and examine the distribution of concentrations at fixed mass in § 5. In § 6, we explore the physical effects that might cause anomalously high measurements of concentration for some clusters, and present our conclusions in § 7.

One of the key points we emphasize is that the clusters in this compiled sample have their masses and concentrations measured using a variety of different methods: strong lensing, weak lensing, X-ray temperatures, line of sight velocity distributions, and the caustic method. In several cases, a cluster's mass and concentration are measured using multiple methods that yield different results, and it is these discrepancies that are of interest. Throughout this paper, we adopt a spatially flat cosmological model dominated by cold dark matter and a cosmological constant ($\Omega_{\rm m0} = 0.3$, $\Omega_{\Lambda 0} = 0.7$, $h = 0.7$).

2 DEFINITION OF THE CONCENTRATION PARAMETER

Cosmological simulations of structure formation suggest that dark matter halos, independent of mass or cosmology, follow the density profile given by Navarro et al. (1996, 1997). The spherically averaged NFW profile is given by

$$\rho(r) = \frac{\rho_{\rm s}}{(r/r_{\rm s})(1+r/r_{\rm s})^2} \ , \tag{1}$$

where $\rho_{\rm s}$ is a characteristic density and $r_{\rm s}$ is the scale radius, which describes the transition point where the density profile turns over from $\rho \propto r^{-1}$ to $\rho \propto r^{-3}$. The mass contained within radius r of an NFW halo that produces gravitational lensing of the background sources is

$$M(\leqslant r) = 4\pi\Sigma_{\rm crit}\kappa_{\rm s} r_{\rm s}^2 \left[\ln(1+x) - \frac{x}{1+x}\right] \ , \tag{2}$$

where $x \equiv r/r_{\rm s}$ and $\Sigma_{\rm crit}$ is the critical surface mass density, defined as

$$\Sigma_{\rm crit} \equiv \frac{c^2}{4\pi G}\frac{D_s}{D_l D_{ls}} \ , \tag{3}$$

which depends on the angular diameter distances $D_{l,s,ls}$ from the observer to the lens, to the source, and from the lens to the source, respectively. The scale convergence is $\kappa_{\rm s} = \rho_{\rm s} r_{\rm s}/\Sigma_{\rm crit}$ (Bartelmann 1996).

The concentration parameter of a halo is the ratio of its virial radius to its scale radius, and is representative of the halo's central density. In much of the literature discussing cluster concentrations, two distinct definitions of the virial radius are commonly used. First, the virial radius may be defined as the radius r_{200} at which the average halo density is 200 times the critical density at the halo redshift. In this case, the concentration is denoted as $c_{200} \equiv r_{200}/r_{\rm s}$. In an alternative convention, the virial radius is defined as the radius $r_{\rm vir}$ at which the average halo density is $\Delta_{\rm vir}(z)$ times the mean density at the halo redshift z, where $\Delta_{\rm vir}(z) = (18\pi^2 + 82x - 39x^2)/(1+x)$ and $x \equiv \Omega_m(z) - 1$ (Hu & Kravtsov 2003). The resultant halo concentration is $c_{\rm vir} \equiv r_{\rm vir}/r_{\rm s}$.

For ease of comparison with other work, we will henceforth report all measurements in terms of both definitions of virial radius: c_{200} and the corresponding halo mass $M_{200} \equiv M(\leqslant r_{200})$, and $c_{\rm vir}$ and the corresponding $M_{\rm vir} \equiv M(\leqslant r_{\rm vir})$.

3 OBSERVATIONAL SAMPLE

To determine the observed relation between concentration and virial mass for galaxy clusters, we compile a sample of all known observationally-determined concentrations and the corresponding virial masses. The bulk of our sample is drawn from pre-existing data in the literature, but we also incorporate new concentration and mass determinations for 10 strong lensing clusters. This compilation presents the most complete sample of observed cluster concentrations and virial masses yet assembled; in total, our sample consists of 182 unique measurements for 100 galaxy clusters.

3.1 New Concentrations for 10 Strong Lensing Clusters

Comerford et al. (2006) used the strong lensing arcs observed in 10 galaxy clusters to fit elliptical NFW dark matter density profiles to each cluster. Using their best-fit scale radius and scale convergence parameters, as well as the observed cluster and arc redshifts, we determine a concentration and mass for each lens, shown in Table 1. We compute errors in concentration and mass based on the errors derived for the best-fit NFW parameters. As detailed in Comerford et al. (2006) these errors are quite small (and likely underestimate the true error) because they apply to one particular model and do not reflect degeneracies between models.

In particular, for several lensing clusters, the best-fit mass distribution is bi-modal and due to the difficulty of converting these mass models accurately to a single NFW parameterization to derive the concentration, we retain in our sample only clusters that are well defined by a primary single dark matter halo. Our fits to the clusters ClG 2244−02, 3C 220.1, MS 2137.3−2353, MS 0451.6−0305, and MS 1137.5+6625 fulfill this criterion, more than doubling the number of existing cluster concentration and mass measurements, with errorbars, from strong lensing.

Two of the clusters from Comerford et al. (2006), ClG 0054−27 and Cl 0016+1609, do not have published arc redshifts, preventing us from determining the cluster's critical surface mass density (Equation 3) and therefore the virial mass or the concentration parameter. Instead, we assume a ratio of angular diameter distances $D_s/D_{ls} = 1$ to calculate the concentrations and masses for these two clusters, reported in Table 1. We exclude these two clusters, however, from the analysis that follows.

3.2 Compiling Published Observations

We combine our concentration and mass measurements with those in the literature to create a complete sample of observed galaxy cluster concentrations and virial masses. The mass distributions of these clusters are fit using a variety of observational methods, and in many cases a cluster is independently fit by different authors using different methods. The assumption of spherical or axial symmetry of the halo often figures prominently in mass calculations. We briefly outline below each of the methods employed in the determination of a dark matter halo's mass distribution.

Table 1. New cluster concentrations and masses determined via strong lensing.

Cluster	Lens[a]	c_{200}	M_{200} $(10^{14}\,M_\odot)$	$c_{\rm vir}$	$M_{\rm vir}$ $(10^{14}\,M_\odot)$
ClG 2244−02		4.3 ± 0.4	4.5 ± 0.9	5.2 ± 0.5	5.2 ± 1.1
Abell 370	G1	4.8 ± 0.2	9.0 ± 1.0	5.8 ± 0.3	$10. \pm 1$
	G2	5.2 ± 0.3	6.7 ± 0.7	6.3 ± 0.3	7.7 ± 0.8
3C 220.1		4.3 ± 0.2	3.1 ± 0.3	5.0 ± 0.2	3.5 ± 0.3
MS 2137.3−2353		13 ± 1	2.9 ± 0.4	16 ± 1	3.2 ± 0.4
MS 0451.6−0305		5.5 ± 0.3	18 ± 2	6.4 ± 0.3	$20. \pm 2$
MS 1137.5+6625		3.3 ± 0.2	6.5 ± 0.7	3.8 ± 0.2	7.2 ± 0.8
ClG 0054−27[b]	G1	1.2 ± 0.1	0.42 ± 0.07	1.5 ± 0.1	0.52 ± 0.09
	G2	2.1 ± 0.1	0.95 ± 0.12	2.5 ± 0.1	1.1 ± 0.1
Cl 0016+1609[b]	DG 256	2.1 ± 0.1	1.1 ± 0.2	2.5 ± 0.1	1.3 ± 0.2
	DG 251	2.3 ± 0.1	0.51 ± 0.06	2.7 ± 0.1	0.59 ± 0.07
	DG 224	3.1 ± 0.2	3.1 ± 0.4	3.6 ± 0.2	3.6 ± 0.4
Cl 0939+4713	G1	4.5 ± 0.3	0.71 ± 0.11	5.4 ± 0.4	0.81 ± 0.12
	G2	3.7 ± 0.3	1.1 ± 0.2	4.5 ± 0.3	1.2 ± 0.2
	G3	4.5 ± 0.2	1.4 ± 0.1	5.4 ± 0.3	1.6 ± 0.2
ZwCl 0024+1652	#362	4.6 ± 0.2	3.1 ± 0.1	5.5 ± 0.3	2.6 ± 0.3
	#374	4.3 ± 0.2	3.7 ± 0.5	5.1 ± 0.3	4.2 ± 0.5
	#380	3.4 ± 0.2	2.7 ± 0.3	4.1 ± 0.2	3.2 ± 0.3

[a] See Comerford et al. (2006) for lens identification.

[b] Because these cluster arcs have no published redshifts, we calculate the concentration and mass assuming $D_s/D_{ls} = 1$. Note that we do not use these concentration and mass determinations in our observed concentration-mass fit.

Strong lensing (SL) — Strong lensing typically occurs when the projected surface mass density in the inner regions of a cluster is sufficiently high to produce one or more distorted images of a single background galaxy. The observed positions, orientations, and magnifications of the lensed images are used to constrain the mass distribution of the cluster lens. The integrated mass determined in the inner regions of a cluster from strong lensing effects is often systematically higher than that determined using X-ray data, leading to higher values of the estimated concentration parameter compared to the average galaxy cluster that is not a lens. This effect is due to the fact that lensing clusters and in particular those that exhibit strong lensing tend to preferentially sample the high mass end of the cluster mass function.

Weak lensing (WL) — The gravitational tidal field caused by a mass distribution produces elongated, tangential distortions of background objects. These weak distortions are observed at large radii from the center of lensing clusters and their statistical analyses provide a direct measure of the density profile of the cluster lens at intermediate to large radii.

Combined weak lensing and strong lensing (WL+SL) — If both weak and strong lensing measurements of a cluster are used in combination, they can be used to effectively break the mass-sheet degeneracy (Schneider & Seitz 1995) that often plagues solitary strong or weak lensing mass measurements. Therefore, the combination of strong and weak lensing can provide a more accurate and calibrated mass distribution for a cluster.

X-ray temperature — The hot gas in galaxy clusters emits X-rays via bremsstrahlung radiation and atomic line emission. The surface brightness distribution and the measured cluster temperature can be used to determine the density profile. Combining the temperature and density information yields the cluster mass. However, the X-ray technique for mass determination assumes that the intra-cluster gas is distributed in a spherically symmetric fashion and is in hydrostatic equilibrium (Evrard et al. 1996). These assumptions may be untenable; for example, observed buoyant bubbles near the cores of galaxy clusters suggest the hot gas may not be strictly in hydrostatic equilibrium (e.g., Churazov et al. 2001).

Line of sight velocity distribution (LOSVD) — The LOSVD for a cluster is a function relating the number of cluster galaxies with their line of sight velocities. This function is parameterized by velocity moments, which can be measured observationally (for example, the second moment of the LOSVD is the square of the line of sight velocity dispersion). Combining these results with the Jeans equation, assuming spherical symmetry, determines the potential and therefore the density profile of the cluster itself.

Caustic method (CM) — When the line of sight velocity is plotted against the projected clustercentric radius, member galaxies in a cluster align in a distinctively flaring pattern. The edges of these flares are called caustics and demarcate the cluster infall region (Kaiser 1987). Based on the location and amplitude of these caustics, we can infer the cluster potential and therefore the mass of a cluster. However, this technique relies upon the assumptions of spherical symmetry and does not adequately take into account the non-linearities in structure formation.

A variety of definitions are used in the literature for the virial radius, and for consistency we employ the Hu & Kravtsov (2003) formula to convert all concentrations and masses to our preferred convention of (c_{200}, M_{200}) and ($c_{\rm vir}$, $M_{\rm vir}$). We also convert all the data to a flat ΛCDM cosmological model ($\Omega_{\rm m0} = 0.3$, $\Omega_{\Lambda 0} = 0.7$, $h = 0.7$). The entire sample is presented in Table A-1, which we use to define an observed cluster concentration-mass relation.

4 THE OBSERVED CONCENTRATION-MASS RELATION

To discern the trend between concentration and mass, we first cull our sample down to only those concentrations that have corresponding virial mass estimates and that have published errors in both quantities. This narrows our sample down to 62 clusters.

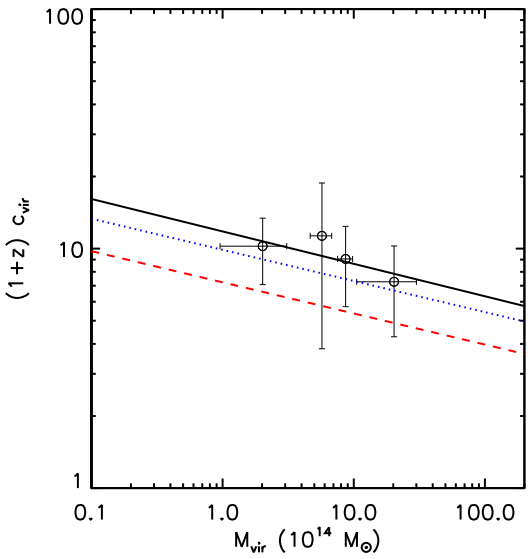

Figure 1. Observed cluster concentrations and virial masses, binned by mass with approximately equal numbers of clusters in each bin. Data points illustrate the mean concentration and mass of each bin, and the solid line is our best fit. The slope of our fit is consistent with fits from simulations, Hennawi et al. (2007) (dotted blue line) and Bullock et al. (2001) (dashed red line), though our normalization is somewhat higher.

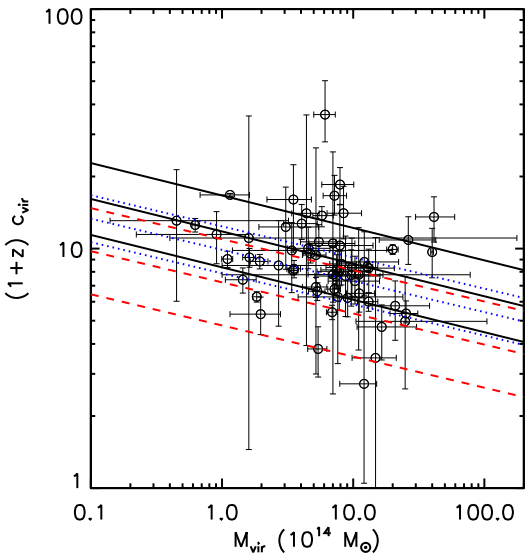

Figure 2. Observed cluster concentrations and virial masses, as well as the best-fit power law $c_{\rm vir} = \frac{14.8}{(1+z)}(M_{\rm vir}/M_\star)^{-0.14}$ (solid black line). The outer two solid black lines depict the 1-σ scatter $\Delta(\log c_{\rm vir}) \sim 0.15$. Also plotted are two $c-M$ relations from simulated clusters: the Hennawi et al. (2007) $c_{\rm vir} = \frac{12.3}{(1+z)}(M_{\rm vir}/M_\star)^{-0.13}$ (dotted blue line, with outer dotted blue lines as 1-σ scatter) and the Bullock et al. (2001) $c_{\rm vir} = \frac{9}{(1+z)}(M_{\rm vir}/M_\star)^{-0.13}$ (dashed red line, with outer dashed red lines as 1-σ scatter).

Several clusters have multiple, distinct measurements of their concentration and virial mass, leading them to be over-represented in our sample in comparison to clusters with a single measurement. To address this problem, we take the median value of the concentration and its corresponding virial mass to be representative of a cluster with multiple measurements. This is done consistently in our analysis.

As the distribution of cluster concentrations is so broad, we bin the data into four mass bins with approximately equal numbers of clusters in each bin for a more effective comparison. We determine the mean and standard deviation of the cluster concentrations (normalized to $z = 0$) and masses in each bin, then fit a power law,

$$c_{\rm vir} = \frac{c_0}{1+z}\left(\frac{M_{\rm vir}}{M_\star}\right)^{\alpha}, \quad (4)$$

where c_0 and α are constants, z is the cluster redshift, and the mass normalization is taken to be $M_\star = 1.3 \times 10^{13} h^{-1} M_\odot$ as in the simulations. The best fit we obtain is $c_{\rm vir} = \frac{14.8\pm6.1}{(1+z)}(M_{\rm vir}/M_\star)^{-0.14\pm0.12}$, shown in Figure 1. We compare our fit to the $c-M$ relations inferred from dissipationless N-body simulations of ΛCDM cosmic structure formation, which are $c_{\rm vir} = \frac{9}{(1+z)}(M_{\rm vir}/M_\star)^{-0.13}$ from Bullock et al. (2001) and $c_{\rm vir} = \frac{12.3}{(1+z)}(M_{\rm vir}/M_\star)^{-0.13}$ from Hennawi et al. (2007).

Our fit has approximately the same slope as the simulations, but a somewhat larger normalization by a factor of 1.6 compared to Bullock et al. (2001) and a factor of 1.2 compared to Hennawi et al. (2007) simulations.

Our finding of a slope α consistent with simulations is significant, because previous studies of observed clusters have not found this agreement. Fits to X-ray clusters of mass $> 10^{14} M_\odot$ have found $\alpha \sim 0$, or an approximately constant concentration-mass relation (Pointecouteau et al. 2005; Vikhlinin et al. 2006). In the opposite extreme, studies of X-ray galaxy groups and poor clusters

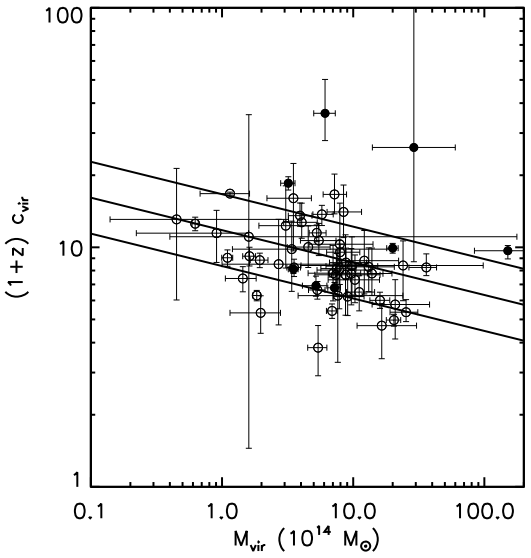

Figure 3. Observed cluster concentrations and virial masses derived from lensing (filled circles) and X-ray (open circles) measurements. For reference, the solids lines depict the best-fit power law to our complete sample and its 1-σ scatter. The lensing concentrations appear systematically higher than the X-ray concentrations, and a Kolmogorov-Smirnov test confirms that the lensing results likely belong to a different distribution.

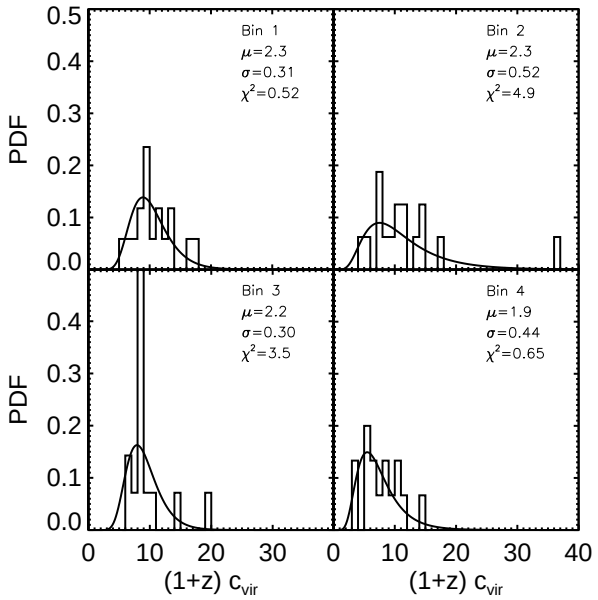

Figure 4. Log-normal fits to normalized histograms of observed cluster concentrations, binned by mass. The mass ranges are $M_{\rm vir} < 4 \times 10^{14} M_\odot$, $4 \times 10^{14} M_\odot < M_{\rm vir} < 7.3 \times 10^{14} M_\odot$, $7.3 \times 10^{14} M_\odot < M_{\rm vir} < 12 \times 10^{14} M_\odot$, and $M_{\rm vir} > 12 \times 10^{14} M_\odot$ for bin 1 to bin 4, respectively. For each mass bin the expectation value μ, standard deviation σ, and χ^2 of the best-fit log-normal function are also given.

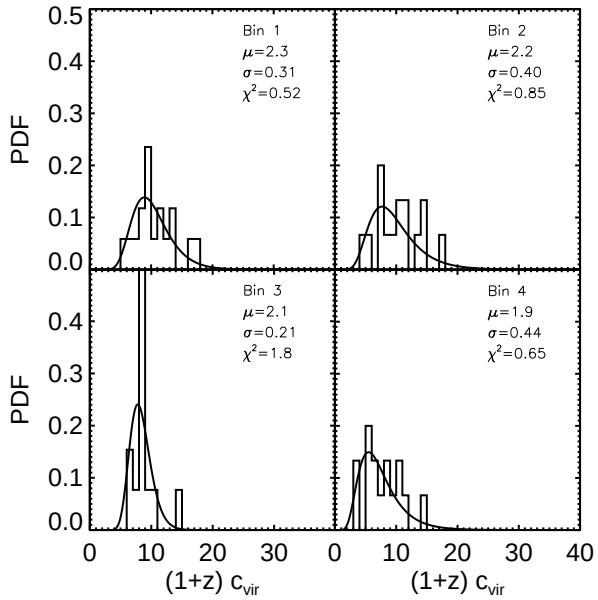

Figure 5. As Fig. 4, but with concentrations greater than 2-σ from the expectation value omitted. This excluded the highest concentration cluster in bin 2 and in bin 3. The resultant fits improved by up to a factor of 6 in χ^2.

with lower virial masses in the range of $\sim 10^{13}\,M_\odot$ find steep slopes of $\alpha = -0.226$ (Gastaldello et al. 2006) and $\alpha = -0.44$ (Sato et al. 2000). Finally, the Buote et al. (2006) sample of X-ray galaxy systems ranging in mass from $10^{13} M_\odot$ to $10^{15} M_\odot$ has a slope of $\alpha = -0.172$.

Both observations and simulations find a large scatter in concentration for a given virial mass, which is likely due to the variation in halo collapse epochs and histories (Bullock et al. 2001). Comparing our best fit to the unbinned clusters, shown in Figure 2, we find a 1-σ scatter of $\Delta(\log c_{\rm vir}) \sim 0.15$ in our relation. The simulations have scatters of ~ 0.18 in Bullock et al. (2001) and ~ 0.098 in Hennawi et al. (2007) (calculated from data courtesy of J. Hennawi). However, we cannot directly compare these to the observationally derived scatters due to the differing systematics.

We note that the concentrations of clusters determined from lensing methods (weak, strong, and a combination of the two) are systematically higher than the concentrations determined by other methods. Figure 3 shows the distribution of lensing concentrations relative to X-ray concentrations; a Kolmogorov-Smirnov test finds only a 28% probability that the two are in fact derived from the same parent distribution.

A similar, though less pronounced, effect has been found in numerical simulations of clusters. Hennawi et al. (2007) identified lensing clusters from their simulated sample by using ray tracing to compute strong lensing cross sections for each cluster, and found that the simulated strong lensing clusters have on average 34% higher concentrations than the total simulated cluster population. In our observed sample, we find a larger fraction: about 55% higher concentrations on average for observed strong lensing clusters.

Why are lensing concentrations systematically higher than X-ray concentrations? Several known physical effects are implicated in explaining this discrepancy. The X-ray method of determining a mass distribution depends on the assumption of hydrostatic equilibrium, which breaks down for unrelaxed clusters. As a result, X-ray measurements may underpredict concentrations for unrelaxed systems such as clusters undergoing mergers.

In particular, if non-thermal sources of pressure support are present and significant, for example due to the presence of a magnetic field on small scales in the inner regions of a cluster, the assumption of hydrostatic equilibrium will tend to underestimate the total mass and hence yield a systematically lower value for the concentration. Loeb & Mao (1994) argue that for the cluster Abell 2218, a factor of about $2-3$ discrepancy in the strong lensing determined mass and the X-ray determined mass (under the assumption of hydrostatic equilibrium) enclosed within 200 kpc can be explained with the existence of an equi-partition magnetic field. This effect alone could likely close the gap between X-ray and lensing concentrations.

In addition to underpredicted X-ray concentrations, overpredicted lensing concentrations could also contribute to the discrepancy in concentration estimates. In particular, lensing concentrations can be inflated due to the effects of halo triaxiality, substructure along the line of sight, and adiabatic contraction in the dark matter due to the collapse of baryons in the inner regions of halos.

It is impossible to observationally determine a distant halo's three-dimensional shape, and most mass-finding techniques assume a spherical halo. However, a spherical halo model fit to a triaxial cluster, if projected along the major axis, would overestimate both the cluster's concentration and its virial mass (Gavazzi 2005; Oguri et al. 2005). If a halo were significantly elongated along the line of sight, its concentration could be overestimated up to 50% and its virial mass estimation could double (Corless & King 2006). Methods now exist to estimate the shape of a dark matter halo from the observed intracluster gas (Lee & Suto 2003).

Structure along the line of sight to the cluster can also contribute to a higher estimated concentration. Simulations of King & Corless (2007) determined that multiple subhalos close to the line of sight are most effective at increasing the concentration estimate of the main halo. Neglecting large-scale structure, as most

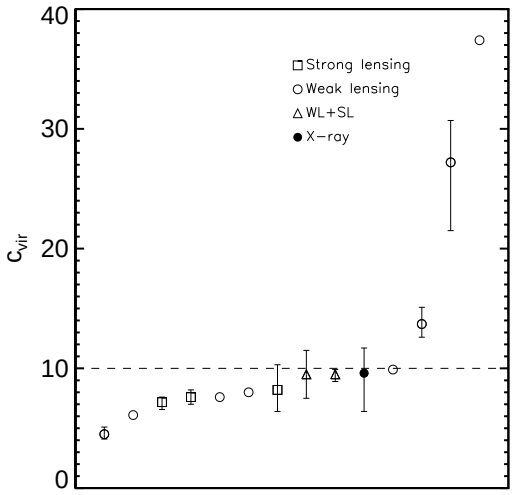

Figure 6. Observed concentrations for the cluster Abell 1689, ordered from lowest to highest. Only weak lensing measurements produce the anomalously high $c_{\rm vir} > 10$ concentrations (dashed line).

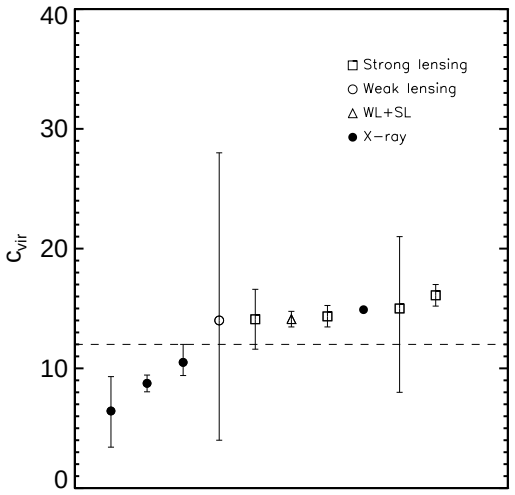

Figure 7. Observed concentrations for the cluster MS 2137.3−2353, ordered from lowest to highest. Note that all of the smaller values of concentration $c_{\rm vir} < 12$ (dashed line), which are more consistent with predictions from observed and simulated $c - M$ relations, are from X-ray measurements.

halo mass models do, can artificially and substantially inflate concentration estimates.

Finally, adiabatic contraction in the halo core could substantially increase a cluster's concentration, as argued by Gnedin et al. (2004). The dissipative collapse of baryons in the centers of dark matter halos induces a steepening of the dark matter density profile in these regions. This steepening will systematically increase the concentrations. Adiabatic contraction could explain why our observed lensing concentrations are yet higher than the simulated cluster lens concentrations in our comparison. The Hennawi et al. (2007) simulated lensing clusters are products of dissipationless simulations, whereas observed clusters have presumably undergone adiabatic contraction and a corresponding steepening in the density profile, yielding a higher value for the concentration.

5 CONCENTRATIONS FOR FIXED HALO MASS

Numerical simulations further indicate that concentrations for fixed halo mass are log-normally distributed. To test this hypothesis for observed clusters, we examine the clusters grouped into four mass bins, as detailed in § 4. We then fit a log-normal function to the distribution of concentrations in each bin. For our $x = (1+z)c_{\rm vir}$, the log-normal probability density function (PDF) is

$$f(x;\mu,\sigma) = \frac{1}{\sqrt{2\pi}\sigma x}\exp\left(\frac{-(\ln x-\mu)^2}{2\sigma^2}\right) , \quad (5)$$

where μ and σ are the expectation value and standard deviation.

The panels in Figure 4 show the best-fit log-normal functions to each mass bin, as well as the expectation value, standard deviation, and χ^2 for each fit. The concentrations appear to be consistent with a log-normal distribution, with the exception of a couple of high concentration clusters that lie beyond the tail of the distribution. To determine how well the bulk of concentrations, without the outliers, is fit by a log-normal distribution, we omit all concentrations greater than 2-σ from the expectation value. This cut eliminates one cluster from bin 2 (top row, right in Fig. 4) and one from bin 3 (bottom row, left in Fig. 4).

The resultant fits, shown in Figure 5, have improved in goodness of fit to the data by a factors of 6 and 2 in χ^2 for bin 2 and bin 3, respectively. All four bins are now well-fit by a log-normal function, suggesting that the vast majority of observed clusters follow a log-normal distribution, but with a few outliers with substantially higher concentrations.

These outliers are ZwCl 0024+1652 (in bin 2) and MS 2137.3−2353 (in bin 3), and their anomalously high concentrations are well documented in the literature. Possible explanations for these high concentrations are presented in the next section.

6 ANOMALOUSLY HIGH CONCENTRATION CLUSTERS

Three clusters stand out for their anomalously high concentrations, which are several sigma higher than the predicted concentration-mass relations. They are the lensing clusters ZwCl 0024+1652 ($c_{\rm vir} = 26$; Kneib et al. 2003), Abell 1689, and MS 2137.3−2353.

Although there are only lensing measurements of the ZwCl 0024+1652 concentration, multiple strong lensing, weak lensing, combined strong and weak lensing, and X-ray measurements have been made of the concentrations and virial masses of both Abell 1689 and MS 2137.3−2353. Many of these individual measurements are even consistent with concentration-mass relations, leading us to ask whether the anomalously high concentrations are indeed real, and what the physical explanation for these high concentrations might be.

Figure 6 illustrates the range of concentrations measured for the cluster Abell 1689. Strikingly, if not for the weak lensing measurements, this cluster would have a rather typical range of concentrations. Apparently some systematic effect causes the weak lensing concentrations to be inflated relative to concentrations inferred

via other methods. For instance, the weak lensing signal could be more sensitive to substructure close to the line of sight, causing concentration overestimates, as discussed in § 4.

We see an analogous effect in MS 2137.3−2353, shown in Figure 7. Here, all of the smaller, unsurprising concentration values are the result of X-ray measurements. Lensing measurements produce most of the anomalously high concentrations.

As discussed in § 4, X-ray concentrations can be systematically low for clusters that do not conform to the assumption of hydrostatic equilibrium. And, lensing concentrations can be elevated due to projection effects, substructure, or adiabatic contraction. We expect lensing concentrations to be greater than X-ray concentrations, but it is yet unclear whether the anomalously high lensing concentrations of these three clusters are real.

This concern has been addressed for each of the three anomalously high concentration clusters. The high lensing concentration of MS 2137.3−2353 may be explained by an elongated halo with its major axis close to the line of sight (Gavazzi 2005). Also, ZwCl 0024+1652 exhibits prominent substructure that may account for its high concentration estimates. For example, Kneib et al. (2003) identify a main clump with high concentration as well as a secondary, low concentration clump, while this paper (Table 1) fits three $c_{\rm vir} \sim 5$ clumps to ZwCl 0024+1652.

Perhaps the most progress has been made in explaining Abell 1689's concentration, which has been measured to be as high as $c_{\rm vir} = 37.4$ (Halkola et al. 2006) but has come down to a consensus of $c_{\rm vir} \sim 6 - 8$ (Limousin et al. 2006) due to careful, detailed modeling including an unprecedented large number of strong lensing constraints.

7 SUMMARY AND CONCLUSIONS

We have presented a comprehensive set of observed galaxy cluster concentrations and virial masses, including new concentration estimates for 10 strong lensing clusters. With this data, we fit the dependence of the concentration parameter with virial mass to a power law to compare with the relation obtained in simulations. The main results of this analysis are:

1. The observed cluster concentrations and virial masses are best fit by the power law $c_{\rm vir} = \frac{14.8 \pm 6.1}{(1+z)} (M_{\rm vir}/M_\star)^{-0.14 \pm 0.12}$ with $M_\star = 1.3 \times 10^{13}\, h^{-1}\, M_\odot$. The slope is consistent with the value of -0.13 found by simulations, in contrast to previous observational studies which found a steeper slope or no slope at all. The normalization of our best fit is at least 20% higher than the normalizations found by simulations. We suspect that adiabatic contraction and a steepening of the dark matter density profile in response to the collapse of baryons in real clusters offers a likely explanation for this systematic offset.

2. Cluster concentrations derived from lensing analyses are systematically higher than concentrations derived via X-ray temperatures. We find that observed strong lensing clusters have concentrations 55% higher, on average, than the rest of the cluster population, a larger factor than found in simulations. The discrepancy between lensing and X-ray concentrations is likely due to some combination of X-ray concentrations underpredicted for unrelaxed clusters and lensing concentrations overpredicted due to halo triaxiality, structure along the line of sight, and adiabatic contraction.

3. For fixed mass, the majority of observed clusters are distributed log-normally in concentration, with a few exceptions. The log-normal distribution is predicted by simulations, but has not been measured observationally prior to this work. The exceptions to this log-normal distribution are two clusters well-known for their anomalously high concentration measurements.

4. The three clusters with the highest concentration measurements have been well studied, and the physical effects (such as halo elongation, substructure, and adiabatic contraction) behind these large concentrations are better understood. These effects need to be accounted for with careful modeling.

Although our observed concentration-mass relation for galaxy clusters is reasonably consistent (albeit with a higher normalization) with present simulations, the Millennium simulation will offer the best comparison set to the observed relation reported here. This simulation will offer ample statistics spanning all four mass bins for a direct comparison with our data.

ACKNOWLEDGMENTS

J.M.C. and P.N. acknowledge insightful and useful discussions with Matthias Bartelmann. We also benefited from exchanges at the concentration discussion group at the KITP workshop on applications of gravitational lensing. J.M.C. acknowledges support by a National Science Foundation Graduate Research Fellowship.

REFERENCES

Allen S. W., Schmidt R. W., Fabian A. C., Ebeling H., 2003, MNRAS, 342, 287
Andersson K. E., Madejski G. M., 2004, ApJ, 607, 190
Bardeau S., Kneib J.-P., Czoske O., Soucail G., Smail I., Ebeling H., Smith G. P., 2005, A&A, 434, 433
Bartelmann M., 1996, A&A, 313, 697
Broadhurst T., et al., 2005, ApJ, 621, 53
Broadhurst T., Takada M., Umetsu K., Kong X., Arimoto N., Chiba M., Futamase T., 2005, ApJ, 619, L143
Bullock J., Kolatt T., Sigad Y., Somerville R., Kravtsov A., Klypin A., Primack J., Dekel A., 2001, MNRAS, 321, 559
Buote D. A., Gastaldello F., Humphrey P. J., Zappacosta L., Bullock J. S., Brighenti F., Mathews W. G., 2006, ArXiv Astrophysics e-prints
Buote D. A., Humphrey P. J., Stocke J. T., 2005, ApJ, 630, 750
Buote D. A., Lewis A. D., 2004, ApJ, 604, 116
Churazov E., Brüggen M., Kaiser C. R., Böhringer H., Forman W., 2001, ApJ, 554, 261
Clowe D., 2003, in Bowyer S., Hwang C.-Y., eds, Astronomical Society of the Pacific Conference Series Wide-Field Weak Lensing Cluster Mass Reconstructions. pp 271–+
Clowe D., Schneider P., 2001a, ArXiv Astrophysics e-prints
Clowe D., Schneider P., 2001b, A&A, 379, 384
Clowe D., Schneider P., 2002, A&A, 395, 385
Comerford J. M., Meneghetti M., Bartelmann M., Schirmer M., 2006, ApJ, 642, 39
Corless V., King L., 2006, ArXiv Astrophysics e-prints
David L. P., Nulsen P. E. J., McNamara B. R., Forman W., Jones C., Ponman T., Robertson B., Wise M., 2001, ApJ, 557, 546
Evrard A. E., Metzler C. A., Navarro J. F., 1996, ApJ, 469, 494
Gastaldello F., Buote D. A., Humphrey P. J., Zappacosta L., Bullock J. S., Brighenti F., Mathews W. G., 2006, ArXiv Astrophysics e-prints
Gavazzi R., 2002, New Astronomy Review, 46, 783
Gavazzi R., 2005, A&A, 443, 793

Gavazzi R., Fort B., Mellier Y., Pelló R., Dantel-Fort M., 2003, A&A, 403, 11
Gnedin O. Y., Kravtsov A. V., Klypin A. A., Nagai D., 2004, ApJ, 616, 16
Halkola A., Seitz S., Pannella M., 2006, MNRAS, 372, 1425
Hennawi J. F., Dalal N., Bode P., Ostriker J. P., 2007, ApJ, 654, 714
Hu W., Kravtsov A. V., 2003, ApJ, 584, 702
Kaiser N., 1987, MNRAS, 227, 1
Kelson D. D., Zabludoff A. I., Williams K. A., Trager S. C., Mulchaey J. S., Bolte M., 2002, ApJ, 576, 720
Khosroshahi H. G., Maughan B. J., Ponman T. J., Jones L. R., 2006, MNRAS, 369, 1211
King L., Corless V., 2007, MNRAS, 374, L37
King L. J., Clowe D. I., Schneider P., 2002, A&A, 383, 118
Kling T. P., Dell'Antonio I., Wittman D., Tyson J. A., 2005, ApJ, 625, 643
Kneib J., Hudelot P., Ellis R. S., Treu T., Smith G. P., Marshall P., Czoske O., Smail I., Natarajan P., 2003, ApJ, 598, 804
Lee J., Suto Y., 2003, ApJ, 585, 151
Lewis A. D., Buote D. A., Stocke J. T., 2003, ApJ, 586, 135
Limousin M., Richard J., Kneib J. ., Jullo E., Fort B., Soucail G., Elíasdóttir A., Natarajan P., Smail I., Ellis R. S., Czoske O., Hudelot P., Bardeau S., Ebeling H., Smith G. P., 2006, ArXiv Astrophysics e-prints
Loeb A., Mao S., 1994, ApJ, 435, L109
Łokas E. L., Mamon G. A., 2003, MNRAS, 343, 401
Łokas E. L., Wojtak R., Gottlöber S., Mamon G. A., Prada F., 2006, MNRAS, 367, 1463
Markevitch M., Vikhlinin A., Forman W. R., Sarazin C. L., 1999, ApJ, 527, 545
Maughan B. J., Jones C., Jones L. R., Van Speybroeck L., 2006, ArXiv Astrophysics e-prints
McLaughlin D. E., 1999, ApJ, 512, L9
Medezinski E., Broadhurst T., Umetsu K., Coe D., Benitez N., Ford H., Rephaeli Y., Arimoto N., Kong X., 2006, ArXiv Astrophysics e-prints
Molikawa K., Hattori M., Kneib J.-P., Yamashita K., 1999, A&A, 351, 413
Moore B., Quinn T., Governato F., Stadel J., Lake G., 1999, MNRAS, 310, 1147
Navarro J., Frenk C., White S., 1996, ApJ, 462, 563
Navarro J., Frenk C., White S., 1997, ApJ, 490, 493
Navarro J. F., Hayashi E., Power C., Jenkins A. R., Frenk C. S., White S. D. M., Springel V., Stadel J., Quinn T. R., 2004, MNRAS, 349, 1039
Oguri M., Takada M., Umetsu K., Broadhurst T., 2005, ApJ, 632, 841
Pointecouteau E., Arnaud M., Kaastra J., de Plaa J., 2004, A&A, 423, 33
Pointecouteau E., Arnaud M., Pratt G. W., 2005, A&A, 435, 1
Pratt G. W., Arnaud M., 2005, A&A, 429, 791
Rines K., Diaferio A., 2006, AJ, 132, 1275
Rines K., Geller M. J., Kurtz M. J., Diaferio A., 2003, AJ, 126, 2152
Sato S., Akimoto F., Furuzawa A., Tawara Y., Watanabe M., Kumai Y., 2000, ApJ, 537, L73
Schmidt R. W., Allen S. W., 2006, ArXiv Astrophysics e-prints
Schneider P., Seitz C., 1995, A&A, 294, 411
Vikhlinin A., Kravtsov A., Forman W., Jones C., Markevitch M., Murray S. S., Van Speybroeck L., 2006, ApJ, 640, 691
Vikhlinin A., Markevitch M., Murray S. S., Jones C., Forman W., Van Speybroeck L., 2005, ApJ, 628, 655
Voigt L. M., Fabian A. C., 2006, MNRAS, 368, 518
Wang Y., Xu H., Zhang Z., Xu Y., Wu X.-P., Xue S.-J., Li Z., 2005, ApJ, 631, 197
Williams L. L. R., Saha P., 2004, AJ, 128, 2631
Xu H., Jin G., Wu X.-P., 2001, ApJ, 553, 78
Zekser K. C., White R. L., Broadhurst T. J., Benítez N., Ford H. C., Illingworth G. D., Blakeslee J. P., Postman M., Jee M. J., Coe D. A., 2006, ApJ, 640, 639

APPENDIX A: COMPLETE COMPILATION OF OBSERVED CLUSTER CONCENTRATIONS AND VIRIAL MASSES

Table A-1 contains the full data set of observed cluster concentrations and virial masses used in this paper. We convert all concentrations and masses to our definitions of virial radius (given in § 2) and use $h = 0.7$ throughout. In all, there are 182 unique measurements of 100 clusters.

Table A-1: Cluster concentrations and masses

Cluster	z	Method	c_{200}	M_{200} $(10^{14}\,M_\odot)$	$c_{\rm vir}$	$M_{\rm vir}$ $(10^{14}\,M_\odot)$	Reference
Virgo	0.003	X-ray	2.8 ± 0.7	4.2 ± 0.5	3.8 ± 0.9	5.4 ± 0.9	McLaughlin (1999)
Abell 1060	0.01	LOSVD	$10.6^{+17.1}_{-7.7}$	$3.8^{+0.4}_{-0.7}$	$13.9^{+21.9}_{-10.0}$	$4.4^{+1.1}_{-1.0}$	Łokas et al. (2006)
		X-ray	8.4 ± 0.6		11.1 ± 0.8		Xu et al. (2001)
Abell 262	0.0163	LOSVD	$3.1^{+8.7}_{-2.4}$	$2.1^{+0.2}_{-0.6}$	$4.2^{+11.2}_{-3.2}$	$2.7^{+1.2}_{-1.0}$	Łokas et al. (2006)
		X-ray	6.7 ± 0.5	0.929 ± 0.082	8.9 ± 0.7	1.100 ± 0.106	Gastaldello et al. (2006)
		X-ray	5.29 ± 0.43		7.03 ± 0.55		Vikhlinin et al. (2005)
		X-ray	12.9 ± 1.1		16.8 ± 1.4		Xu et al. (2001)
Abell 194	0.018	CM	6.27	1.09	8.30	1.30	Rines et al. (2003)
MKW 4	0.0200	X-ray	9.4 ± 0.7	0.54 ± 0.027	12.3 ± 0.8	0.624 ± 0.034	Gastaldello et al. (2006)
		X-ray	3.85 ± 0.22	1.11 ± 0.15	5.17 ± 0.28	1.37 ± 0.20	Vikhlinin et al. (2005)
Abell 3581	0.0218	X-ray	$9.81^{+6.30}_{-5.40}$	$0.39^{+2.23}_{-0.27}$	$12.8^{+8.1}_{-6.9}$	$0.45^{+2.76}_{-0.31}$	Voigt & Fabian (2006)
Abell 1367	0.022	CM	16.9	5.46	21.9	6.11	Rines et al. (2003)
Abell 1656	0.023	CM	10.0	11.2	13.1	12.9	Rines et al. (2003)
		LOSVD	7.0	11.8 ± 0.3	9.3	13.9 ± 4	Łokas & Mamon (2003)
Abell 539	0.029	CM	14.7	3.63	19.0	4.09	Rines et al. (2003)
Abell 2199	0.030	CM	7.47	4.67	9.80	5.47	Rines et al. (2003)
		LOSVD	$7.79^{+11.26}_{-6.02}$	$6.0^{+1.5}_{-1.8}$	$10.2^{+14.4}_{-7.8}$	$7.0^{+3.3}_{-2.4}$	Łokas et al. (2006)
		LOSVD	4	5	5	6	Kelson et al. (2002)
		X-ray	8.2 ± 0.4		10.7 ± 0.5		Xu et al. (2001)
		X-ray	10		13		Markevitch et al. (1999)
AWM 4	0.0317	X-ray	6.8 ± 0.6	1.375 ± 0.146	8.9 ± 0.8	1.619 ± 0.182	Gastaldello et al. (2006)
Abell 496	0.0329	CM	14.0	3.13	18.1	3.53	Rines et al. (2003)
		LOSVD	$6.9^{+12.9}_{-4.8}$	$4.5^{+0.3}_{-0.7}$	$9.1^{+16.4}_{-6.2}$	$5.2^{+1.0}_{-1.1}$	Łokas et al. (2006)
		X-ray	10.4 ± 0.6		13.5 ± 0.8		Xu et al. (2001)
		X-ray	6		8		Markevitch et al. (1999)
Abell 2063	0.0337	X-ray	5.1 ± 0.3		6.8 ± 0.4		Xu et al. (2001)
2A 0335+096	0.0347	X-ray	$8.18^{+18.83}_{-7.20}$	$1.4^{+115.5}_{-1.0}$	$10.7^{+23.9}_{-9.3}$	$1.6^{+175.4}_{-1.2}$	Voigt & Fabian (2006)
Abell 2052	0.0348	X-ray	9.7 ± 0.7		12.6 ± 0.9		Xu et al. (2001)
MKW 9	0.0382	X-ray	5.41 ± 0.67	1.20 ± 0.30	7.14 ± 0.86	1.44 ± 0.38	Pointecouteau et al. (2005)
		X-ray	5.4 ± 0.7	1.20	7.1 ± 0.9	1.44	Pratt & Arnaud (2005)
Abell 3571	0.039	X-ray	4.9 ± 0.2		6.5 ± 0.3		Xu et al. (2001)
Abell 576	0.04	CM	10.9	9.51	14.1	10.85	Rines et al. (2003)
RXJ0137	0.0409	X-ray	6.34	0.99	8.32	1.17	Rines & Diaferio (2006)
		X-ray	4.9 ± 2.4		6.5 ± 3.1		Buote & Lewis (2004)
Abell 160	0.0432	X-ray	10.14	0.91	13.16	1.04	Rines & Diaferio (2006)
Abell 1983	0.0442	X-ray	3.83 ± 0.71	1.59 ± 0.61	5.10 ± 0.91	1.97 ± 0.82	Pointecouteau et al. (2005)
Abell 119	0.0446	CM	6.29	4.07	8.25	4.81	Rines et al. (2003)
		X-ray	2.55	2.36	3.45	3.06	Rines & Diaferio (2006)
		X-ray	3.3 ± 0.2		4.4 ± 0.3		Xu et al. (2001)
MKW 3S	0.045	X-ray	6.4 ± 0.7		8.4 ± 0.9		Xu et al. (2001)
Abell 168	0.0451	CM	5.19	4.30	6.84	5.17	Rines et al. (2003)
		X-ray	7.69	2.24	10.03	2.61	Rines & Diaferio (2006)
Abell 4059	0.0478	X-ray	4.8 ± 0.2		6.3 ± 0.3		Xu et al. (2001)
Abell 3558	0.048	LOSVD	$1.9^{+4.0}_{-1.2}$	$9.0^{+0.3}_{-2.3}$	$2.6^{+5.1}_{-1.6}$	$12.1^{+3.0}_{-4.2}$	Łokas et al. (2006)
		X-ray	4.0 ± 0.2		5.3 ± 0.3		Xu et al. (2001)
Abell 2717	0.049	X-ray	4.6 ± 0.3	1.510 ± 0.089	6.0 ± 0.3	1.839 ± 0.122	Gastaldello et al. (2006)
		X-ray	4.21 ± 0.25	1.57 ± 0.19	5.58 ± 0.32	1.92 ± 0.25	Pointecouteau et al. (2005)
		X-ray	4.2 ± 0.3	1.57	5.6 ± 0.4	1.92	Pratt & Arnaud (2005)
Abell 3562	0.0499	X-ray	5.4 ± 0.8		7.1 ± 1.0		Xu et al. (2001)
Hydra A	0.0538	X-ray	12.3 ± 0.18	1.02 ± 0.41	15.9 ± 0.23	1.15 ± 0.47	David et al. (2001)
Abell 85	0.0557	X-ray	4.50	3.36	5.93	4.08	Rines & Diaferio (2006)
		X-ray	7.5 ± 0.6		9.8 ± 0.8		Xu et al. (2001)
Sersic 159 03	0.0564	X-ray	$6.16^{+3.42}_{-2.79}$	$2.3^{+7.9}_{-1.4}$	$8.05^{+4.34}_{-3.56}$	$2.7^{+10.0}_{-1.7}$	Voigt & Fabian (2006)
Abell 2319	0.0564	X-ray	5.8 ± 0.2		7.6 ± 0.3		Xu et al. (2001)
Abell 133	0.0569	X-ray	4.77 ± 0.42	4.41 ± 0.59	6.28 ± 0.53	5.33 ± 0.77	Vikhlinin et al. (2005)
Abell 1991	0.0586	X-ray	5.78 ± 0.35	1.63 ± 0.18	7.56 ± 0.45	1.94 ± 0.22	Pointecouteau et al. (2005)
		X-ray	$5.7^{+0.4}_{-0.3}$	1.63	$7.5^{+0.5}_{-0.4}$	1.94	Pratt & Arnaud (2005)

Table A-1 – *Continued*

Cluster	z	Method	c_{200}	M_{200} $(10^{14}\,M_\odot)$	$c_{\rm vir}$	$M_{\rm vir}$ $(10^{14}\,M_\odot)$	Reference
		X-ray	6.40 ± 0.46	1.65 ± 0.24	8.35 ± 0.58	1.94 ± 0.30	Vikhlinin et al. (2005)
Abell 3266	0.0594	X-ray	3.9 ± 0.2		5.2 ± 0.3		Xu et al. (2001)
Abell 3158	0.0597	LOSVD	$2.5^{+0.57}_{-1.8}$	$11.4^{+1.7}_{-3.0}$	$3.3^{+7.2}_{-2.4}$	$14.8^{+6.5}_{-5.0}$	Łokas et al. (2006)
Abell 1795	0.063	X-ray	$4.45^{+0.86}_{-0.77}$	$7.48^{+2.32}_{-1.58}$	$5.86^{+1.09}_{-0.98}$	$9.07^{+3.03}_{-2.03}$	Schmidt & Allen (2006)
		X-ray	$4.28^{+2.23}_{-2.41}$	$8.9^{+54.5}_{-5.6}$	$5.64^{+2.84}_{-3.09}$	$10.8^{+74.4}_{-7.0}$	Voigt & Fabian (2006)
		X-ray	4.82 ± 0.26	8.38 ± 0.79	6.32 ± 0.33	10.10 ± 1.01	Vikhlinin et al. (2005)
		X-ray	7.6 ± 0.3		9.9 ± 0.4		Xu et al. (2001)
Abell 644	0.0704	X-ray	4.6 ± 0.9	7	6.0 ± 1.2	8	Buote et al. (2005)
		X-ray	4.6 ± 0.2		6.0 ± 0.3		Xu et al. (2001)
Abell 401	0.0748	X-ray	4.2 ± 0.3		5.5 ± 0.4		Xu et al. (2001)
Abell 3112	0.0750	X-ray	$7.06^{+3.62}_{3.23}$	$2.9^{+13.5}_{-1.9}$	$9.14^{+2.82}_{-3.05}$	$3.4^{+16.4}_{-2.2}$	Voigt & Fabian (2006)
Abell 2029	0.0767	X-ray	$6.64^{+0.34}_{-0.38}$	$7.66^{+0.77}_{-0.58}$	$8.60^{+0.42}_{-0.48}$	$8.97^{+0.94}_{-0.71}$	Schmidt & Allen (2006)
		X-ray	$4.38^{+1.64}_{-1.76}$	$20.^{+57}_{-16}$	$5.74^{+2.08}_{-2.24}$	$24^{+74}_{-20.}$	Voigt & Fabian (2006)
		X-ray	6.00 ± 0.30	10.81 ± 1.08	7.80 ± 0.38	12.76 ± 1.33	Vikhlinin et al. (2005)
		X-ray	4.4 ± 0.9	12 ± 2	5.8 ± 1.1	15 ± 3	Lewis et al. (2003)
		X-ray	8.4 ± 0.6		10.8 ± 0.8		Xu et al. (2001)
RXJ1159.8+5531	0.081	X-ray	8.3 ± 2.1	0.787 ± 0.533	10.6 ± 2.6	0.908 ± 0.686	Gastaldello et al. (2006)
		X-ray	2.63 ± 0.43		3.51 ± 0.55		Vikhlinin et al. (2005)
Abell 1651	0.0825	X-ray	4.9 ± 0.2		6.4 ± 0.3		Xu et al. (2001)
Abell 2597	0.0852	X-ray	5.86 ± 0.50	3.00 ± 0.33	7.59 ± 0.63	3.54 ± 0.42	Pointecouteau et al. (2005)
		X-ray	6.7 ± 0.6		8.7 ± 0.8		Xu et al. (2001)
Abell 478	0.088	X-ray	$3.92^{+0.36}_{-0.33}$	$13.1^{+2.3}_{-2.1}$	$5.13^{+0.45}_{-0.41}$	$16.0^{+3.0}_{-2.6}$	Schmidt & Allen (2006)
		X-ray	$2.88^{+2.02}_{-\rightarrow 2.88}$	$34^{+\rightarrow\infty,a}_{-26}$	$3.81^{+2.56}_{-\rightarrow 3.81}$	$43^{+\rightarrow\infty,a}_{-33}$	Voigt & Fabian (2006)
		X-ray	4.22 ± 0.39	10.8 ± 1.8	5.52 ± 0.49	13.1 ± 2.3	Pointecouteau et al. (2005)
		X-ray	5.33 ± 0.39	10.53 ± 1.51	6.92 ± 0.49	12.51 ± 1.88	Vikhlinin et al. (2005)
		X-ray	4.2 ± 0.4	11	5.5 ± 0.5	13	Pointecouteau et al. (2004)
		X-ray	$3.67^{+0.31}_{-0.35}$	$18.4^{+4.8}_{-2.4}$	$4.82^{+0.39}_{-0.44}$	$22.6^{+6.2}_{-3.1}$	Allen et al. (2003)
		X-ray	6.7 ± 0.4		8.6 ± 0.5		Xu et al. (2001)
PKS0745−191	0.103	X-ray	$5.86^{+1.56}_{-1.07}$	$11.82^{+4.70}_{-3.55}$	$7.55^{+1.95}_{-1.34}$	$13.89^{+5.85}_{-1.07}$	Schmidt & Allen (2006)
		X-ray	$5.46^{+3.22}_{-2.88}$	$9.7^{+52.2}_{-8.5}$	$7.05^{+4.04}_{-3.63}$	$11^{+67}_{-10.}$	Voigt & Fabian (2006)
		X-ray	5.12 ± 0.40	10.0 ± 1.2	6.62 ± 0.50	11.9 ± 1.5	Pointecouteau et al. (2005)
		X-ray	$3.83^{+0.52}_{-0.27}$	$18.6^{+3.5}_{-4.0}$	$5.00^{+0.66}_{-0.34}$	$22.7^{+4.5}_{-5.1}$	Allen et al. (2003)
RXJ1416.4+2315	0.137	X-ray	11.2 ± 4.5	3.1 ± 1.0	14.1 ± 5.6	3.5 ± 1.3	Khosroshahi et al. (2006)
Abell 1068	0.1375	X-ray	3.69 ± 0.26	5.68 ± 0.49	4.77 ± 0.33	6.90 ± 0.65	Pointecouteau et al. (2005)
Abell 1413	0.143	X-ray	$4.44^{+0.78}_{-0.75}$	$9.31^{+2.69}_{-1.77}$	$5.69^{+0.97}_{-0.94}$	$11.11^{+3.45}_{-2.23}$	Schmidt & Allen (2006)
		X-ray	5.82 ± 0.50	6.50 ± 0.65	7.41 ± 0.62	7.59 ± 0.82	Pointecouteau et al. (2005)
		X-ray	4.42 ± 0.24	10.67 ± 1.17	5.66 ± 0.30	12.73 ± 1.47	Vikhlinin et al. (2005)
Abell 2204	0.152	WL	6.3	12^{+3}_{-2}	8.0	14^{+3}_{-2}	Clowe & Schneider (2002)
		WL	4.3		5.5		Clowe & Schneider (2001a)
		X-ray	$9.75^{+2.92}_{-2.16}$	$7.48^{+2.63}_{-1.80}$	$12.2^{+3.60}_{-2.67}$	$8.44^{+3.14}_{-2.12}$	Schmidt & Allen (2006)
		X-ray	4.59 ± 0.37	11.8 ± 1.3	5.86 ± 0.46	14.0 ± 1.7	Pointecouteau et al. (2005)
Abell 907	0.1603	X-ray	5.21 ± 0.60	6.28 ± 0.63	6.61 ± 0.75	7.37 ± 0.82	Vikhlinin et al. (2005)
Abell 1689	0.18	SL	6.0 ± 0.5	30.	7.6 ± 0.6	35	Halkola et al. (2006)
		SL	$5.70^{+0.34}_{-0.50}$	$130.^{+88}_{-57}$	$7.18^{+0.42}_{-0.62}$	151^{+104}_{-67}	Zekser et al. (2006)
		SL	$6.5^{+1.9}_{-1.6}$	34^{+1}_{-2}	$8.2^{+2.1}_{-1.8}$	$40.^{+1}_{-1}$	Broadhurst et al. (2005)
		WL	30.4		37.4		Halkola et al. (2006)
		WL	$22.1^{+2.9}_{-4.7}$		$27.2^{+3.5}_{-5.7}$		Medezinski et al. (2006)
		WL	$3.5^{+0.5}_{-0.3}$	$14.1^{+6.3}_{-4.7}$	$4.5^{+0.6}_{-0.4}$	$17.1^{+7.8}_{-5.8}$	Bardeau et al. (2005)
		WL	$11.0^{+1.14}_{-0.90}$	17.3 ± 1.7	$13.7^{+1.4}_{-1.1}$	19.3 ± 2.0	Broadhurst et al. (2005)
		WL	7.9		9.9		Clowe (2003)
		WL	4.8	8.50	6.1	10.0	King et al. (2002)
		WL	6		8		Clowe & Schneider (2001b)
		WL	6.0		7.6		Clowe & Schneider (2001a)
		WL+SL	$7.6^{+0.3}_{-0.5}$	23	$9.5^{+0.4}_{-0.6}$	26	Halkola et al. (2006)
		WL+SL	7.6 ± 1.6	13.2 ± 2	9.5 ± 2.0	15.1 ± 2	Limousin et al. (2006)
		X-ray	$7.7^{+1.7}_{-2.6}$		$9.6^{+2.1}_{-3.2}$		Andersson & Madejski (2004)
Abell 383	0.188	X-ray	$3.76^{+0.53}_{-0.68}$	$6.62^{+2.56}_{-1.34}$	$4.78^{+0.65}_{-0.84}$	$7.95^{+3.28}_{-1.68}$	Schmidt & Allen (2006)

Table A-1 – *Continued*

Cluster	z	Method	c_{200}	M_{200} $(10^{14}\,M_\odot)$	$c_{\rm vir}$	$M_{\rm vir}$ $(10^{14}\,M_\odot)$	Reference
		X-ray	6.41 ± 0.57	4.10 ± 0.47	8.03 ± 0.70	4.72 ± 0.57	Vikhlinin et al. (2005)
MS 0839.9+2938	0.194	X-ray	6.5 ± 0.1	6.1	8.1 ± 0.1	7.0	Wang et al. (2005)
MS 0451.5+0250	0.202	X-ray	3.79	129	4.80	154	Molikawa et al. (1999)
Abell 963	0.206	X-ray	$4.39^{+0.88}_{-0.88}$	$7.47^{+3.05}_{-1.80}$	$5.53^{+1.07}_{-1.08}$	$8.81^{+3.84}_{-2.21}$	Schmidt & Allen (2006)
		X-ray	$5.72^{+0.78}_{-1.07}$	$7.04^{+1.96}_{-1.26}$	$7.16^{+0.95}_{-1.31}$	$8.14^{+2.43}_{-1.51}$	Allen et al. (2003)
RXJ0439.0+0520	0.208	X-ray	$6.66^{+1.53}_{-1.21}$	$3.97^{+1.78}_{-1.19}$	$8.30^{+1.87}_{-1.48}$	$4.54^{+2.13}_{-1.40}$	Schmidt & Allen (2006)
RXJ1504.1−0248	0.215	X-ray	$3.77^{+1.05}_{-1.09}$	$17.5^{+13.5}_{-5.6}$	$4.75^{+1.28}_{-1.34}$	$20.9^{+17.3}_{-6.97}$	Schmidt & Allen (2006)
MS 0735.6+7421	0.216	X-ray	6.85	22	8.51	25	Molikawa et al. (1999)
MS 1006.0+1202	0.221	X-ray	4.19	31	5.26	36	Molikawa et al. (1999)
Abell 2390	0.230	X-ray	2.58 ± 0.19	16.58 ± 1.93	3.28 ± 0.23	20.45 ± 2.57	Vikhlinin et al. (2005)
		X-ray	$3.20^{+1.79}_{-1.57}$	$20.6^{+59.7}_{-11.6}$	$4.04^{+2.18}_{-1.93}$	$24.9^{+79.7}_{-14.4}$	Allen et al. (2003)
Abell 2667	0.233	X-ray	$3.02^{+0.74}_{-0.85}$	$13.6^{+10.6}_{-4.6}$	$3.82^{+0.90}_{-1.04}$	$16.5^{+13.9}_{-5.8}$	Allen et al. (2003)
RXJ2129.6+0005	0.235	X-ray	$4.07^{+2.31}_{-1.97}$	$6.46^{+12.6}_{-3.14}$	$5.09^{+2.80}_{-2.41}$	$7.63^{+16.3}_{-3.83}$	Schmidt & Allen (2006)
MS 1910.5+6736	0.246	X-ray	4.65	8.7	5.78	10.	Molikawa et al. (1999)
Abell 1835	0.252	WL	2.96	$23.8^{+3.5}_{-3.2}$	3.72	$28.8^{+4.2}_{-3.9}$	Clowe & Schneider (2002)
		WL	4.8		5.96		Clowe & Schneider (2001a)
		X-ray	$3.42^{+0.45}_{-0.31}$	$21.2^{+4.62}_{-5.03}$	$4.28^{+0.55}_{-0.37}$	$25.3^{+5.78}_{-6.21}$	Schmidt & Allen (2006)
		X-ray	$3.13^{+1.37}_{-1.44}$	24^{+104}_{-16}	$3.93^{+1.66}_{-1.76}$	$29^{+136}_{-20.}$	Voigt & Fabian (2006)
		X-ray	$4.21^{+0.53}_{-0.61}$	$18.2^{+8.4}_{-3.0}$	$5.24^{+0.64}_{-0.74}$	$21.4^{+10.3}_{-3.7}$	Allen et al. (2003)
MS 1455.0+2232	0.259	X-ray	10.9	14	13.2	15	Molikawa et al. (1999)
Abell 611	0.288	X-ray	$5.08^{+1.72}_{-1.61}$	$6.81^{+4.68}_{-2.11}$	$6.24^{+2.06}_{-1.94}$	$7.83^{+5.78}_{-2.53}$	Schmidt & Allen (2006)
		X-ray	$4.58^{+2.36}_{-2.22}$	$9.4^{+16.6}_{-3.9}$	$5.64^{+2.83}_{-2.68}$	11^{+21}_{-5}	Allen et al. (2003)
Zwicky 3146	0.291	X-ray	$2.32^{+2.31}_{-\to 2.32}$	$28.1^{+\to\infty}_{-16.3}$	$2.91^{+2.78}_{-\to 2.91}$	$34.5^{+\to\infty}_{-20.9}$	Schmidt & Allen (2006)
Abell 2537	0.295	X-ray	$4.83^{+2.32}_{-1.59}$	$7.58^{+5.88}_{-3.04}$	$5.93^{+2.78}_{-1.91}$	$8.74^{+7.28}_{-3.64}$	Schmidt & Allen (2006)
MS 1008.1−1224	0.301	X-ray	4.40	34	5.40	39	Molikawa et al. (1999)
MS 2137.3−2353	0.313	SL	13 ± 1	2.9 ± 0.4	16 ± 1	3.2 ± 0.4	This paper
		SL	$11.92^{+0.77}_{-0.74}$	$7.56^{+0.63}_{-0.54}$	$14.34^{+0.91}_{-0.88}$	$8.29^{+0.71}_{-0.61}$	Gavazzi (2005)
		SL	12.5^{+5}_{-6}	7.9	15.0^{+6}_{-7}	8.6	Gavazzi et al. (2003)
		SL	11.7 ± 2.1	7.23 ± 1.90	14.1 ± 2.5	7.93 ± 2.17	Gavazzi (2002)
		WL	12^{+12}_{-8}	$9.3^{+85.4}_{-7.8}$	$14^{+14}_{-10.}$	$10.^{+100.}_{-9}$	Gavazzi et al. (2003)
		WL+SL	11.73 ± 0.55	$7.72^{+0.47}_{-0.42}$	14.11 ± 0.65	$8.47^{+0.53}_{-0.48}$	Gavazzi (2005)
		X-ray	$7.21^{+0.58}_{-0.59}$	$4.70^{+0.81}_{-0.56}$	$8.75^{+0.69}_{-0.71}$	$5.27^{+0.94}_{-0.65}$	Schmidt & Allen (2006)
		X-ray	$5.28^{+2.41}_{-2.52}$	$8.0^{+32.0}_{-4.8}$	$6.44^{+2.87}_{-3.02}$	$9.1^{+39.0}_{-5.6}$	Voigt & Fabian (2006)
		X-ray	$8.71^{+1.22}_{-0.92}$	$4.25^{+0.84}_{-0.88}$	$10.5^{+1.5}_{-1.1}$	$4.72^{+0.96}_{-1.00}$	Allen et al. (2003)
		X-ray	12.4	11	14.9	12	Molikawa et al. (1999)
MACSJ0242.6-2132	0.314	X-ray	$6.69^{+1.23}_{-0.92}$	$4.85^{+1.64}_{-1.31}$	$8.12^{+1.46}_{-1.09}$	$5.47^{+1.92}_{-1.51}$	Schmidt & Allen (2006)
MS 0353.6−3642	0.320	X-ray	4.84	32	5.91	36	Molikawa et al. (1999)
MACSJ2229.8-2756	0.324	X-ray	$7.70^{+3.66}_{-2.62}$	$2.74^{+2.02}_{-1.00}$	$9.30^{+4.34}_{-3.11}$	$3.06^{+2.38}_{-1.15}$	Schmidt & Allen (2006)
MS 1224.7+2007	0.327	X-ray	11.3	9.2	13.5	10.	Molikawa et al. (1999)
MS 1358.4+6245	0.328	X-ray	5.84	26	7.09	29	Molikawa et al. (1999)
ClG 2244−02	0.33	SL	4.3 ± 0.4	4.5 ± 0.9	5.2 ± 0.5	5.2 ± 1.1	This paper
MACSJ0947.2+7623	0.345	X-ray	$5.41^{+1.86}_{-1.51}$	$10.69^{+8.41}_{-4.04}$	$6.54^{+2.20}_{-1.79}$	$12.15^{+10.04}_{-4.71}$	Schmidt & Allen (2006)
MACSJ1931.8-2635	0.352	X-ray	$3.11^{+1.87}_{-1.88}$	$16.2^{+\to\infty,a}_{-8.6}$	$3.81^{+2.22}_{-2.25}$	$19.2^{+\to\infty,a}_{-10.5}$	Schmidt & Allen (2006)
RXJ1532.9+3021	0.3615	X-ray	$2.77^{+2.28}_{-2.28}$	19^{+675}_{-16}	$3.40^{+2.70}_{-2.75}$	23^{+1006}_{-19}	Voigt & Fabian (2006)
MACSJ1532.9+3021	0.363	X-ray	$4.71^{+1.32}_{-1.25}$	$8.46^{+5.96}_{-2.73}$	$5.69^{+1.56}_{-1.47}$	$9.67^{+7.19}_{-3.22}$	Schmidt & Allen (2006)
MS 1512.4+3647	0.372	X-ray	7.82	7.2	9.35	7.9	Molikawa et al. (1999)
MACSJ1720.3+3536	0.391	X-ray	$4.37^{+1.21}_{-0.88}$	$9.01^{+4.63}_{-3.30}$	$5.26^{+1.42}_{-1.04}$	$10.31^{+5.55}_{-3.87}$	Schmidt & Allen (2006)
ZwCl 0024+1652	0.395	WL+SL	22^{+9}_{-5}	$5.7^{+1.1}_{-1.0}$	$26^{+10.}_{-6}$	$6.1^{+1.2}_{-1.1}$	Kneib et al. (2003)
MACSJ0429.6-0253	0.399	X-ray	$7.64^{+1.57}_{-1.10}$	$3.66^{+1.11}_{-0.97}$	$9.09^{+1.84}_{-1.29}$	$4.05^{+1.27}_{-1.10}$	Schmidt & Allen (2006)
MACSJ0159.8-0849	0.405	X-ray	$4.93^{+1.01}_{-1.07}$	$11.59^{+6.29}_{-3.30}$	$5.90^{+1.18}_{-1.25}$	$13.13^{+7.46}_{-3.84}$	Schmidt & Allen (2006)
MS 0302.7+1658	0.426	X-ray	7.39	8.5	8.75	9.4	Molikawa et al. (1999)
MACSJ0329.7-0212	0.450	X-ray	$4.74^{+0.75}_{-0.78}$	$6.62^{+2.57}_{-1.56}$	$5.62^{+0.88}_{-0.91}$	$7.48^{+3.03}_{-1.81}$	Schmidt & Allen (2006)
RXJ1347.5−1145	0.451	WL	15^{+64}_{-10}	27^{+26}_{-14}	18^{+74}_{-12}	29^{+31}_{-15}	Kling et al. (2005)
		X-ray	$4.79^{+0.68}_{-0.37}$	$32.0^{+6.1}_{-8.2}$	$5.68^{+0.79}_{-0.43}$	$36.1^{+7.1}_{-9.5}$	Schmidt & Allen (2006)
		X-ray	$4.37^{+1.39}_{-1.24}$	33^{+48}_{-18}	$5.20^{+1.62}_{-1.45}$	37^{+57}_{-21}	Voigt & Fabian (2006)
		X-ray	$6.34^{+1.61}_{-1.35}$	$23.7^{+14.2}_{-9.3}$	$7.49^{+1.87}_{-1.57}$	$26.3^{+16.3}_{-10.5}$	Allen et al. (2003)
3C 295	0.461	X-ray	$7.79^{+1.04}_{-0.90}$	$3.57^{+0.81}_{-0.65}$	$9.15^{+1.20}_{-0.90}$	$3.93^{+0.92}_{-0.73}$	Schmidt & Allen (2006)

Table A-1 – *Continued*

Cluster	z	Method	c_{200}	M_{200} $(10^{14}\,M_\odot)$	$c_{\rm vir}$	$M_{\rm vir}$ $(10^{14}\,M_\odot)$	Reference
		X-ray	$7.90^{+1.71}_{-1.72}$	$37.6^{+15.9}_{-10.2}$	$9.28^{+1.98}_{-1.99}$	$41.3^{+18.1}_{-11.4}$	Allen et al. (2003)
MACSJ1621.6+3810	0.461	X-ray	$5.97^{+2.95}_{-1.94}$	$7.10^{+5.33}_{-2.90}$	$7.05^{+3.42}_{-2.26}$	$7.91^{+6.25}_{-3.31}$	Schmidt & Allen (2006)
MACSJ1311.0-0311	0.494	X-ray	$4.42^{+1.39}_{-1.05}$	$6.22^{+3.71}_{-2.15}$	$5.22^{+1.60}_{-1.22}$	$7.02^{+4.38}_{-2.49}$	Schmidt & Allen (2006)
MACSJ1423.8+2404	0.539	X-ray	$7.69^{+0.70}_{-0.79}$	$5.28^{+1.13}_{-0.76}$	$8.92^{+0.81}_{-0.91}$	$5.77^{+1.27}_{-0.84}$	Schmidt & Allen (2006)
MS 0015.9+1609	0.546	X-ray	4.37	93.3	5.11	105	Molikawa et al. (1999)
MS 0451.6−0305	0.55	SL	5.5 ± 0.3	18 ± 2	6.4 ± 0.3	$20. \pm 2$	This paper
3C 220.1	0.62	SL	4.3 ± 0.2	3.1 ± 0.3	5.0 ± 0.2	3.5 ± 0.3	This paper
SDSS J1004+4112	0.68	SL	5	3.87	6	4.25	Williams & Saha (2004)
MACSJ0744.9+3927	0.686	X-ray	$4.32^{+1.43}_{-1.06}$	$8.83^{+4.84}_{-3.16}$	$4.95^{+1.61}_{-1.20}$	$9.78^{+5.60}_{-3.58}$	Schmidt & Allen (2006)
MS 1137.5+6625	0.783	SL	3.3 ± 0.2	6.5 ± 0.7	3.8 ± 0.2	7.2 ± 0.8	This paper
ClJ 1226.9+3332	0.89	X-ray	$7.9^{+1.7}_{-1.4}$	$6.8^{+1.6}_{-1.2}$	$8.8^{+1.9}_{-1.5}$	$7.2^{+1.7}_{-1.3}$	Maughan et al. (2006)